



Cite this: *Phys. Chem. Chem. Phys.*,
2015, 17, 32241

Quantum interferences in the photodissociation of $\text{Cl}_2(\text{B})$ in superfluid helium nanodroplets (^4He)_N[†]

Arnau Vilà,^a Miguel González^{*a} and Ricardo Mayol^{*b}

Quantum interferences are probably one of the most fascinating phenomena in chemical physics and, particularly, in reaction dynamics, where they are often very elusive from an experimental perspective. Here, we have theoretically investigated, using a hybrid method recently proposed by us, the dynamics of the formation of confinement quantum interferences in the photodissociation of a Cl_2 molecule ($\text{B} \leftarrow \text{X}$ electronic excitation) embedded in a superfluid helium nanodroplet of different sizes (50–500 ^4He atoms), which is to the best of our knowledge the first time that this type of interference is described in reaction dynamics. Thus, we have widely extended a recent contribution of our group, where interferences were not the main target, identifying the way they are formed and lead to the production of strongly oscillating velocity distributions in the Cl dissociating atoms, and also paying attention to the energy transfer processes involved. This probably corresponds to a rather general behavior in the photodissociation of molecules in helium nanodroplets. We hope that the present study will encourage the experimentalists to investigate this captivating phenomenon, although the technical difficulties involved are very high.

Received 20th June 2015,
Accepted 2nd November 2015

DOI: 10.1039/c5cp03575a

www.rsc.org/pccp

1. Introduction

From a physical perspective, the study of the properties (structure, energy and dynamics) of superfluid helium nanodroplets ($T = 0.37\text{ K}$), (^4He)_N, is a well established and active research area.^{1,2} These systems can act as a low temperature liquid matrix, which allow researchers to carry out high resolution spectroscopic studies of embedded atomic or molecular species, thanks to the chemically inert nature of helium and the superfluid

behavior of helium-4 below a critical temperature ($T = 2.17\text{ K}$). Furthermore, these nanodroplets are also of great interest since they correspond to intermediate size quantum fluid systems, lying between the bulk liquid and molecular clusters.

From a chemical point of view, although the research activity developed to date on the chemical reactivity in helium nanodroplets has been important (see, *e.g.*, ref. 3, 4, and the references cited therein), its intensity is not comparable to the effort carried out in the context of the studies of the physical type. Recently, however, it appears that the chemical interest in these low temperature fluid systems has increased significantly, and this probably occurs thanks to the new possibilities offered by them in the chemical synthesis of novel chemical species. In fact, they allow the synthesis of species that would not be stable in the gas phase as, for instance, some metallic nanoclusters⁵ and nanowires.⁶

On the other hand, little effort has been made to date to explore the reaction dynamics in the (^4He)_N quantum fluid. Thus, as far as we know, only a set of reaction dynamics experiments on the photodissociation of alkyl iodides in (^4He)_N has been reported so far.^{7–9} On the theoretical side, in addition to our recent paper⁴ and the present work on the title system, only one study on reaction dynamics could be found in the literature,¹⁰ which is dedicated to the same problem examined here, but considers both a very different approach and strongly diverse physical conditions (non-superfluid helium nanodroplets at $T = 4\text{ K}$ with

^a Departament de Química Física i IQTC, Universitat de Barcelona, c/Martí i Franquès, 1, 08028 Barcelona, Spain. E-mail: miguel.gonzalez@ub.edu; Fax: +34 93 4021231

^b Departament d'Estructura i Constituents de la Matèria, Universitat de Barcelona, c/Martí i Franquès, 1, 08028 Barcelona, Spain. E-mail: ricardo.mayol@ub.edu; Fax: +34 93 4037063

[†] Electronic supplementary information (ESI) available: Table S1. Initial values of the energies involved in the process. Fig. S1. Snapshots of the squared modulus of the $\text{Cl}_2(\text{B})$ relative coordinate wave packet in the gas phase and also in momentum representation ($N = 500$). Fig. S2. The squared modulus of the $\text{Cl}_2(\text{B})$ wave packet in momentum representation, given in more detail than in Fig. 4 ($N = 300$ and 500). Fig. S3. Time evolution of the energies involved in the process ($N = 100$). Fig. S4. Time evolution of the change and velocity of change of the energies involved in the process ($N = 100$). Movie 1. Time evolution of the squared modulus of the $\text{Cl}_2(\text{B})$ wave packet in coordinate representation and effective potential within the 0.0–3.0 ps interval ($N = 500$). Movie 2. Time evolution of the squared modulus of the $\text{Cl}_2(\text{B})$ wave packet in momentum representation ($N = 500$). See DOI: 10.1039/c5cp03575a



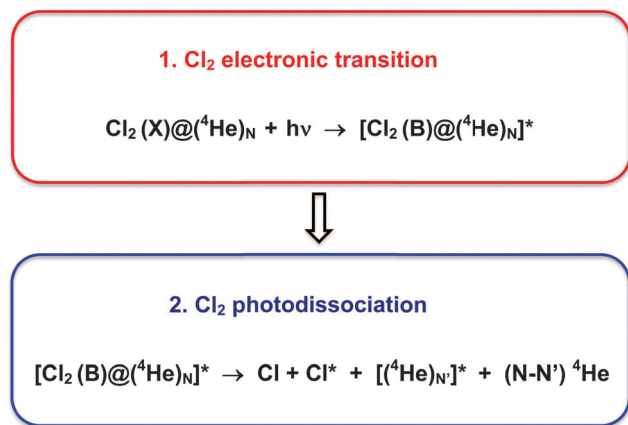


Fig. 1 Schematic representation of the two steps involved in the study of the photodissociation of an embedded Cl₂ molecule in a helium nanodroplet: electronic excitation of Cl₂ from the ground (X) to the excited (B) electronic state followed by the photodissociation of Cl₂(B). Some ⁴He atoms of the nanodroplet are vaporized in step 2.

up to 200 ⁴He atoms). Furthermore, a theoretical investigation on the formation of metal dimers (Cu₂, Ag₂, Au₂) in (⁴He)_N related to the reaction dynamics issues has been reported recently.¹¹

The present study extends and complements our recent investigation on the photodissociation of homonuclear diatomic molecules in superfluid helium nanodroplets (*T* = 0.37 K), where the theoretical method proposed by us was applied for the first time to the photodissociation of a Cl₂ excited embedded molecule (B ← X electronic transition): Cl₂(X)@(⁴He)_N + *hν* → [Cl₂(B)@(⁴He)_N]^{*} → Cl(²P_{3/2}) + Cl(²P_{1/2}) + [(⁴He)_{N'}]^{*} + (N−N') ⁴He, λ ≈ 400 nm (3.10 eV),¹² where the term (N−N') ⁴He merely reflects the total number of vaporized He atoms with *N* maximum = 500 (Fig. 1).

More concretely, in this study we analyze in detail the confinement quantum interferences which are present in this reactive system, and arise from the interaction between the Cl₂(B) molecule and the helium solvent. The interference effects are clearly evident in the final Cl atomic photofragment velocity distributions, which show strongly oscillating patterns with a significant number of well defined peaks for all the nanodroplets (*N* = 50, 100, 200, 300 and 500). Even though interferences are one of the most interesting phenomena in chemical physics¹³ and, of course, in reaction dynamics,^{14,15} they were not the main focus of our previous work,⁴ because of their very specific character and often complex analysis,^{13–15} even for small systems.¹⁶

The paper is organized as follows: in Section II the theoretical methods used are described briefly. Section III is dedicated to the description and analysis of the main results obtained. Summary and conclusions are given in Section IV. Additional useful data can be found in the ESI.†

II. Theoretical methods

An exhaustive description of the theoretical framework used to study the photodissociation dynamics of Cl₂(B) in helium

nanodroplets can be found in ref. 4. However, here we briefly summarize the main features, for the sake of completeness.

Due to the complexity of these systems it is necessary to consider a mean-field approach to investigate the reaction dynamics. Thus, the hybrid theoretical scheme proposed in our previous work,⁴ where the time dependent density functional theory (TDDFT)¹⁷ and the quantum wave packet dynamics¹⁸ methods have been used to describe the evolution of the helium nanodroplet and the relative coordinate of the homonuclear diatomic molecule, respectively, has also been used here. So, we have coupled one of the key procedures employed to describe rather large systems of bosonic liquid helium (from a hundred to thousands of ⁴He atoms) and a common method used in gas phase reaction quantum dynamics, allowing in this way comparison of the theoretical results with the experimental data, when available.

We have neglected the rotational degree of freedom of the molecule as a first approximation to this problem. Nevertheless, this assumption is well justified considering the conditions of the nanodroplets and the rotational constants of the chlorine molecule.⁴ The potential energy surfaces describing the He–Cl₂(X) and He–Cl₂(B) interactions have been taken from ref. 19. They are based on high quality *ab initio* calculations and include some empirical corrections. The potential energy curves of Cl₂(X) and Cl₂(B) are the same as those used in ref. 10 and are also based on high level *ab initio* calculations.²⁰ The starting point for the dynamics requires the determination of the structure of the Cl₂(X)@(⁴He)_N doped nanodroplet, by optimization of the helium density, ρ_{He}, taking into account the helium–Cl₂(X) interaction potential considering the molecule at the ground vibrational level (*v* = 0).

Photodissociation begins with the electronic excitation of the Cl₂(X) molecule (B ← X transition) that we have assumed as a sudden vertical process (the Franck–Condon principle). Hence, both the ground vibrational function of Cl₂(X) and the helium density are kept frozen during the transition and the initial (*t* = 0) wave functions to be propagated in time are defined. Moreover, as in the case of ref. 10 electronic adiabaticity has been considered for the evolution of Cl₂ in the B state, due to the weak coupling of this state with the other electronic states.¹² Some comments on the role that could be played by the A and C excited states in the dynamics are given below.

When the Cl₂(X) molecule is excited by a laser pulse at λ = 400 nm it can be produced in the A, B and C excited states. However, the transition electric dipole moment of the A ← X transition is about one order of magnitude smaller than those for the B ← X and C ← X transitions which are similar to each other.¹² Hence, taking into account the computational difficulties involved in this kind of study, it seems reasonable to neglect the contribution of the A state in the dynamics. Moreover, as the interaction potential between the helium and the excited chlorine molecule is only available for the B state, we have only considered this state in the study. However, in principle, similar dynamics results as those obtained for the B state would be expected for the C state; although the more repulsive character of the Cl₂(C) potential energy curve and its dissociation in ground state chlorine atoms (2Cl(²P_{3/2})) suggest that higher Cl final velocities would be found in this case.



For this theoretical approach the two coupled equations of motion governing the evolution of the helium effective complex wave function, defined as $|\Psi_{\text{He}}(\mathbf{R}_{\text{He}}, t)\rangle^2 \equiv \rho_{\text{He}}(\mathbf{R}_{\text{He}}, t)$, and the relative coordinate wave function (wave packet (WP)), $\varphi_{\text{Cl}_2}(r)$, are respectively as follows:

$$\begin{aligned} i\hbar \frac{\partial}{\partial t} \Psi_{\text{He}}(\mathbf{R}_{\text{He}}) &= \left[-\frac{\hbar^2}{2m_{\text{He}}} \nabla^2 + \int d\mathbf{r} V_{\text{He-Cl}_2(\text{B})}(r, \mathbf{R}_{\text{He}}) |\varphi_{\text{Cl}_2}(r)|^2 \right. \\ &\quad \left. + \frac{\delta \mathcal{E}_{\text{c}}[\rho_{\text{He}}]}{\delta \rho_{\text{He}}} \right] \Psi_{\text{He}}(\mathbf{R}_{\text{He}}) \\ i\hbar \frac{\partial}{\partial t} \varphi_{\text{Cl}_2}(r) &= \left[-\frac{\hbar^2}{m_{\text{Cl}_2}} \frac{\partial^2}{\partial r^2} + \int d\mathbf{R}_{\text{He}} V_{\text{He-Cl}_2(\text{B})}(r, \mathbf{R}_{\text{He}}) \rho_{\text{He}}(\mathbf{R}_{\text{He}}) \right. \\ &\quad \left. + V_{\text{Cl}_2(\text{B})}(r) \right] \varphi_{\text{Cl}_2}(r) \end{aligned} \quad (1)$$

where $\rho_{\text{He}}(\mathbf{R}_{\text{He}})$ and $\mathcal{E}_{\text{c}}[\rho_{\text{He}}]$ are the density and the sum of the correlation and potential energy densities of liquid ^4He , respectively, and the Orsay-Trento phenomenological functional ($T = 0 \text{ K}$)¹⁷ is used to describe the superfluid helium, which is introduced *via* the term $\frac{\delta \mathcal{E}_{\text{c}}[\rho_{\text{He}}]}{\delta \rho_{\text{He}}}$.

As indicated in ref. 4, for computational reasons, the non-local contributions to the correlation energies and the backflow term have not been considered in the Orsay-Trento functional, owing to the major numerical difficulties arising from the consideration of these terms (the use of very small integration steps, depending on the situation). The theoretical study of the dynamics of physicochemical processes involving superfluid (^4He)_N and atoms or molecules has only been possible quite recently and in all cases this approach has been used, leading to a rather good agreement with the experiments.^{21–23} The non-inclusion of the backflow term leads to an increase of the Landau's critical velocity (see Section III.2).

These equations have been solved numerically by discretization of the space in a grid of points for each degree of freedom, using standard methods. Furthermore, negative imaginary potentials (NIPs) have been used so as to avoid artificial reflections of the Cl_2 and helium wave functions at the grid limits (*cf.* ref. 4). The final atomic (Cl) velocity distribution arising from photodissociation has been determined from the asymptotic $(\text{Cl} + \text{Cl}^*)\text{Cl}_2$ relative coordinate wave function, described in momentum representation, before applying the molecular NIP.

III. Results and discussion

III.1 Early times of the photodissociation process and interferences

We have recently studied the dynamics of the photodissociation process $\text{Cl}_2(\text{X})@(^4\text{He})_{\text{N}} + h\nu \rightarrow [\text{Cl}_2(\text{B})@(^4\text{He})_{\text{N}}]^* \rightarrow \text{Cl}(^2\text{P}_{3/2}) + \text{Cl}(^2\text{P}_{1/2}) + (^4\text{He})_{\text{N}'} + (\text{N}-\text{N}')^4\text{He}$ (Fig. 1), which takes place on the picosecond time scale (0.85–2.57 ps for N : 50–500; Table 1);⁴ and in the present paper we focus on the quantum interferences which occur in this reaction which, as indicated

before, were described but not analyzed in our previous contribution because of its complexity. For the time interval of main interest here there is no vaporization of He atoms from the nanodroplets yet. The vaporization process begins, *e.g.*, around 0.56 and 0.70 ps for $N = 50$ and 500, respectively.

The excitation of the embedded Cl_2 molecule from the X ground to the B excited state does not lead directly to the formation of the atomic products, as it happens for the molecule in the gas phase. In fact, differing from what occurs in the gas phase, here the Cl_2 excited molecule is surrounded and temporarily confined by the helium nanodroplet and due to this it takes a substantially larger amount of time to lead to the photodissociation of $\text{Cl}_2(\text{B})$ into $\text{Cl}(^2\text{P}_{3/2}) + \text{Cl}(^2\text{P}_{1/2})$.

Thus, the time delay observed, which has been defined as the time required for the wave packet in coordinate representation, $\text{WP}(r)$, to reach a mean value of the relative distance, $\langle r \rangle$, which is equal to the initial diameter of the nanodroplet (*i.e.*, the photodissociation time definition)⁴ minus the time required for the $\text{WP}(r)$ in the gas phase to reach the same $\langle r \rangle$ value, is in the 0.23–1.38 ps time interval for N : 50–500 (Table 1). In this table the initial radii of the nanodroplets are also given.

The effective or global interaction potential responsible for the evolution of the Cl–Cl separation is equal to the sum of the Cl–Cl interaction potential in the B state and the helium environment– $\text{Cl}_2(\text{B})$ interaction potential. At the beginning of the photodissociation in $(^4\text{He})_{\text{N}}$ (below $t \approx 0.05$ ps), the $\text{Cl}_2(\text{B})$ interaction potential, which is identical to the $\text{Cl}_2(\text{B})$ interaction potential in the gas phase,⁴ clearly dominates over the helium– $\text{Cl}_2(\text{B})$ interaction potential, and the damping of the Cl–Cl interaction mainly occurs because both atoms separate from each other. The situation changes when the dissociating atoms approach the first helium solvation shell, due to the influence of the helium environment. At high enough times the chlorine atoms are far enough from each other and the helium density tends to occupy the space left between them. A detailed analysis of the time evolution of the effective potential will be given along this section, especially illustrating the results shown in Fig. 4, Fig. S3 and Movie 1 (ESI†).

The interaction of the molecule with the helium environment leads to quantum interferences which are evident in the Cl_2 wave packet as described and analyzed below; see also Movies 1 and 2 (ESI†). This leads to a rich structure (oscillations) in the Cl_2 wave function, which at early times is much more evident in the Cl_2 wave packet in momentum representation than in coordinate representation. Oscillations also become evident for the main

Table 1 $[\text{Cl}_2(\text{B})@(^4\text{He})_{\text{N}}]^*$ photodissociation times and associated time delays with respect to the $\text{Cl}_2(\text{B})$ photodissociation in the gas phase

N^a	Photodissoc. time (ps) ⁴	Time delay (ps)
50	0.85	0.23
100	1.14	0.39
200	1.63	0.71
300	2.01	0.98
500	2.57	1.38

^a The initial radii of the nanodroplets for $N = 50, 100, 200, 300$ and 500 are 11.0, 13.0, 15.7, 17.5 and 20.0 Å, respectively.⁴



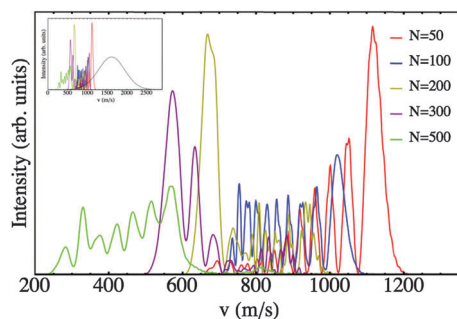


Fig. 2 Velocity distribution of the Cl photofragments produced in the photodissociation of $\text{Cl}_2(\text{B})$ in nanodroplets of different sizes. The gas phase result is shown in the inset (dashed black line) together with the previous results.⁴ Reprinted with permission from *J. Chem. Theory Comput.*, 2015, **11**, 899. Copyright 2015 American Chemical Society.

observable of this system, *i.e.*, the final velocity distribution of the Cl atoms.

In spite of its large conceptual interest, the quantum confinement has been the subject of little attention.^{24,25} Thus, for example, the existence of the related phenomena known as ‘confinement resonances’ was proposed theoretically in a different context (fullerenes that contain endohedral atoms or molecules) in the year 2000, but they remained so elusive experimentally that for many years there was serious doubt about their real existence. They were observed for the first time in 2010 in the photo-ionization spectrum of endohedral Xe in C_{60}^+ .^{24,26}

The main reaction observable here is the velocity distribution of the chlorine photofragments and its dependence on the nanodroplet size. The results obtained for the different droplet sizes are reported in Fig. 2. It can be seen that strong oscillations, resulting from the quantum interferences, are present for all the droplets considered, but not for the photodissociation in the gas phase (*cf.* inset in Fig. 2). This clearly points out that the oscillations are caused by the interaction of the chlorine molecule with the helium environment.

Fig. 3(a) and (b) show the time evolution of the squared modulus of the molecular wave packet in coordinate, $\text{WP}(r)$, and momentum, $\text{WP}(p)$, representations (case $N = 500$), respectively, within the 0.08–0.20 ps interval. Oscillations are found in both representations, although they are much more evident in the second case, and we will focus our attention to the momentum one, since it is directly related to the reaction observable investigated. Additional information on the molecular wave packet time evolution in both the coordinate and momentum representations can be seen in the ESI^\dagger for the nanodroplet with $N = 500$ (Movies 1 and 2, ESI^\dagger respectively). This temporal evolution is in strong contrast to what happens to the free (gas phase) photodissociation of $\text{Cl}_2(\text{B})$ (Fig. S1, ESI^\dagger), as expected.

Schematically, the full process can be divided into three steps: (a) the initial collision of the Cl atoms with the walls of the cavity (initial volume with a radius of ≈ 4.6 Å placed in the nanodroplet and centered in the Cl_2 molecule where no He atoms are found);⁴ (b) the translation of the Cl atoms through the droplet; (c) the arrival of the Cl atoms to the nanodroplet surface and their subsequent departure. Of course, these parts

are not completely decoupled, but the separation is useful because of their different contributions to the final $\text{WP}(p)$ profile.

At the beginning, $t = 0.014$ – 0.015 ps, the momentum space wave packet moves towards high momenta and then goes back with minimal modification of its Gaussian shape (*cf.* Movie 2, ESI^\dagger). In the coordinate representation, this part of the evolution mostly corresponds to the travelling of $\text{WP}(r)$ through the Cl_2 B-state electronic well (*cf.* Movie 1, ESI^\dagger), *i.e.*, it mainly relates to the breaking of the diatomics chemical bond. From the perspective of the quantum interferences, this part does not contribute to any peculiarity.

The appearance of oscillations in the squared modulus of the momentum wave packet starts around $t = 0.08$ ps (Fig. 3(b) and Movie 2, ESI^\dagger). The high momentum components are being decelerated towards lower momentum values, leading to a decrease of the $\text{WP}(p)$ width. At a time of about 0.1 ps the first well-defined oscillating pattern is already formed.

Then, it can be observed that from a time of around 0.2 ps the low-momenta components of $\text{WP}(p)$ start to jiggle, and then shift towards higher values. This process approximately ends at around $t = 0.5$ ps, and makes $\text{WP}(p)$ compressed into an specific range of momenta ($p \sim 40$ – 65 Å^{−1}; *cf.* Movies 1 and 2, ESI^\dagger). From the movie corresponding to the same time period but in position representation (Movie 1, ESI^\dagger), it can be seen that this process correlates with the ‘filling’ of the $\text{Cl}_2(\text{B})$ electronic potential well. This well is clearly seen at the beginning of Movie 1 (ESI^\dagger).

That is to say, some helium density starts to occupy the space placed between the two chlorine atoms, in this way making the global potential experienced by the chlorine atoms less attractive. The contribution of the electronic potential well of $\text{Cl}_2(\text{B})$ to the global or effective potential is negligible with respect to the chlorine–helium repulsive potential at around $t = 0.46$ ps, because the two chlorine atoms are very far from each other (*cf.* Movie 1, ESI^\dagger). So the evolution observed in the low-momenta components of $\text{WP}(p)$ is a consequence of the helium pushing of the remaining part of $\text{WP}(r)$ placed in the $\text{Cl}_2(\text{B})$ electronic well. From this situation the helium environment confines each Cl atom from both sides along the Cl–Cl molecular photodissociation axis.

At longer times the passage of the Cl atoms through the nanodroplet takes place, which implies different time values, depending on the nanodroplet size: ~ 1.5 and 2.1 ps for $N = 300$ and 500 , respectively. During this time interval $\text{WP}(p)$ evolves gradually toward lower momenta, although the force exerted by the helium fluid makes no substantial change in the shape of $\text{WP}(p)$ in a considerable part of this interval. Concerning the wave packet $\text{WP}(r)$, it progresses in the dynamical effective potential energy well of the effective interaction potential energy, which now is essentially coincident with the helium–chlorine atom interaction potential energy (solvation potential energy), due to the negligible contribution of the Cl–Cl interaction potential energy. This dynamic potential energy well depends on time, due to the changes of the helium density, and the progress of $\text{WP}(r)$ is similar to that of a ‘particle evolving in a moving box’ (see Movie 1 (ESI^\dagger)).



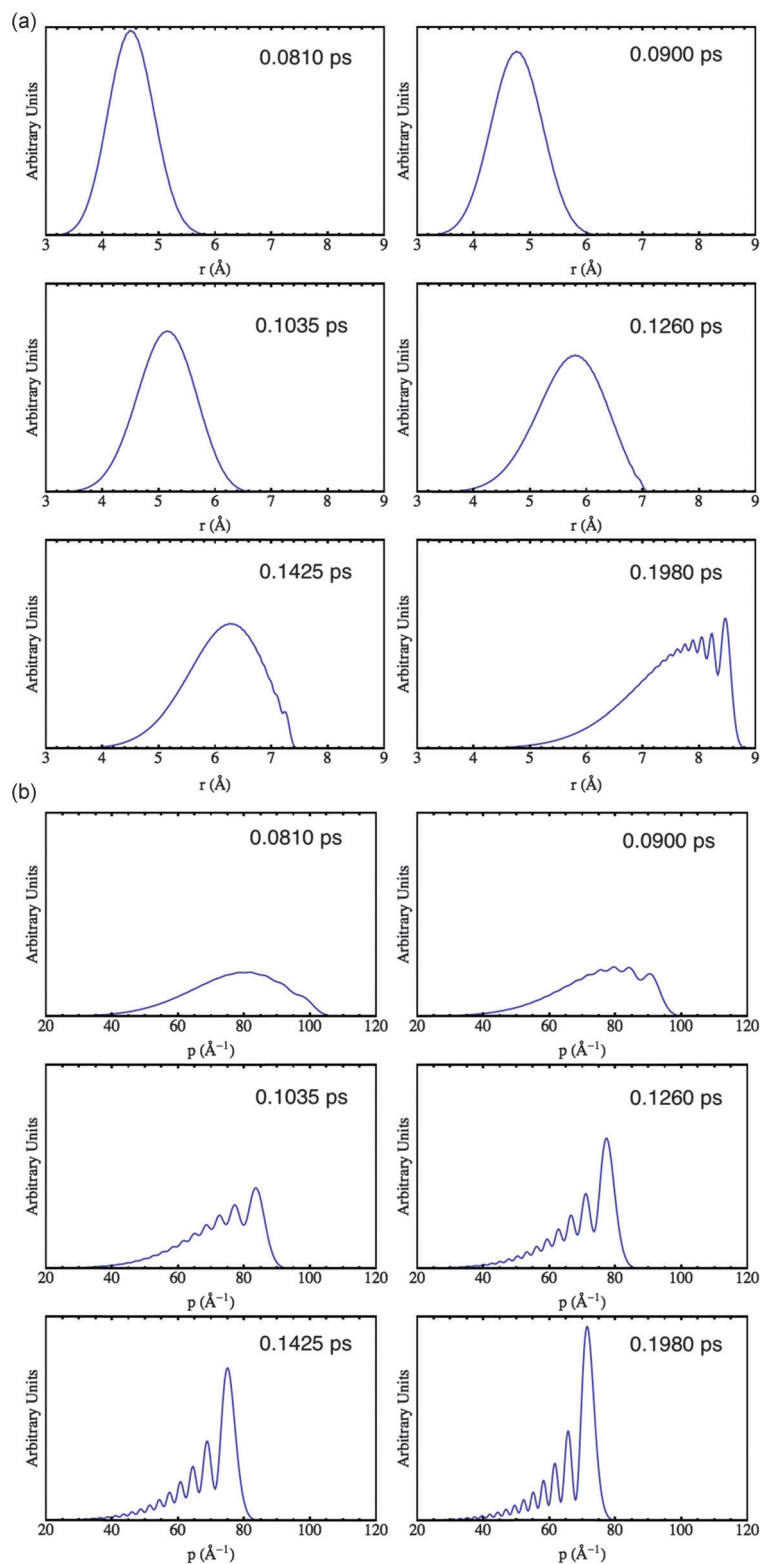


Fig. 3 (a) Snapshots of the evolution of the squared modulus of the $\text{Cl}_2(\text{B})$ relative coordinate wave packet for the nanodroplet of 500 ^4He atoms. (b) The same as Fig. 2(a) but for the wave packet in momentum representation.

For the small and moderately large nanodroplets examined here, the minimal mean velocity of each chlorine atom reached inside the helium nanodroplet occurs when they are about to

reach the surface, and it achieves values around 1050, 910, 740, 640 and 500 m s^{-1} for $N = 50, 100, 200, 300$ and 500, respectively (*cf.* Fig. S1, ESI† of ref. 4). These velocities are



clearly above the Landau's critical velocity in superfluid bulk helium, which has an experimental value of $\approx 58 \text{ m s}^{-1}$ (0.58 \AA ps^{-1}),^{27,28} while a theoretical value of 94 m s^{-1} is obtained when the backflow term is not considered in the Orsay–Trento functional.²¹

However, if the solvent was superfluid bulk liquid or much bigger droplets than the ones considered here, we would expect that, at a given time, the mean value of the velocity of each Cl atom would reach the Landau's critical velocity, as this property has also been observed in nanodroplets with $N \geq 1000$ under softer energy conditions of the dopants.²¹ After reaching this critical speed, the moving effective potential well and $\text{WP}(r)$ would be fully adapted to each other, and would lead to a $\text{WP}(p)$ centered at the corresponding momentum of that critical velocity.

Finally, a variation in the shape of $\text{WP}(p)$ takes place when the dissociating atoms reach the nanodroplet surface,⁴ due to the change in the shape of the effective potential well produced by the large anisotropy of the helium around the chlorine impurities. In Fig. 4 we have plotted the effective potential wells for the nanodroplets with $N = 300$ and 500 and the square modulus of $\text{WP}(p)$'s corresponding to the same times; and the $\text{WP}(p)$'s are given in more detail in Fig. S2 (ESI†). These graphics clearly show the contribution of the nanodroplet surface to the quantum interferences since, although the depth of the effective potential well is always different, its shape changes when the dissociating atoms reach the nanodroplet surface. These potential wells present two high walls with a zone in between where $\text{WP}(r)$ is placed.

During the atomic trip through the nanodroplet, the slope of the effective potential well points towards the direction of the

motion, *i.e.*, to large values of the relative coordinate. This profile arises from the fact that in the direction of motion (increasing r) the helium is compressed, increasing its density and this leads to both a deeper potential well and a larger slope in the potential wall profile. In contrast, in the opposite direction (decreasing r) the helium fills the empty space left by the atomic impurities (lower helium densities).

The shape of the effective potential well reverses when the atomic cavity is opened to the exterior of the nanodroplet. This slightly modifies the momentum space wave packet in comparison with the larger changes observed during the atomic trip inside the nanodroplet, and these slight changes are more evident for the lower momenta, because the dissociating atoms are being attracted by the nanodroplet. Once the atoms are well outside the nanodroplet, the shape of $\text{WP}(p)$ almost does not change while $\text{WP}(r)$ spreads with time, which is consistent with the evolution of a nearly free particle (see also Fig. S1, ESI†).

The former qualitative description of the process accounts to all the nanodroplet sizes considered. The main differences between them arise from the time needed by the atoms to leave the droplet, *i.e.*, in the elapsing time of the penultimate step described above. The formation of the first oscillations in the squared modulus of $\text{WP}(p)$ (Fig. 3(b) and Movie 2, ESI†), which is due to the atomic collision with the first helium solvation layer is almost quantitatively coincident for all cases (Fig. 5); the differences are larger for $N = 50$ since the molecule is never fully solvated.

In spite of the differences in the surface curvature of the nanodroplets, the contribution of the surface to the interferences appears to be similar for all of them. Thus, the dynamical step that mainly influences the final shape of the interferences probably results from the trip of the atomic impurities through the nanodroplet, which leads to the main differences observed in the final Cl velocity distributions.

III.2 Understanding the birth of the interferences

Here we will obtain a deeper insight into the origin of the oscillations in the momentum wave packet including the analysis on the energy fluxes involved. The initial oscillations are produced in the 0.08–0.20 ps time interval, where the pattern is well defined. The mechanism of formation of oscillations can be inferred from Fig. 6 and also from Movies 1 and 2 (ESI†). Thus, at each

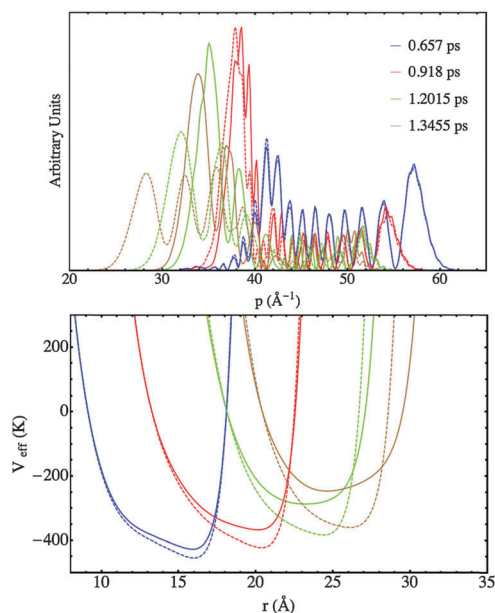


Fig. 4 Squared modulus of the $\text{Cl}_2(\text{B})$ wave packet in momentum representation (up) and effective potential (down), at some time values for which the Cl atoms are travelling inside the nanodroplet; and also when they are relatively close to the nanodroplet surface ($t = 1.346 \text{ ps}$). Two nanodroplet sizes are considered: $N = 300$ (solid line) and $N = 500$ (dashed line).

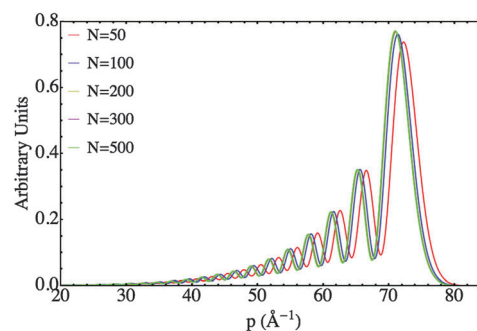


Fig. 5 Squared modulus of the $\text{Cl}_2(\text{B})$ wave packets in momentum representation at $t = 0.198 \text{ ps}$ for different nanodroplet sizes (N).



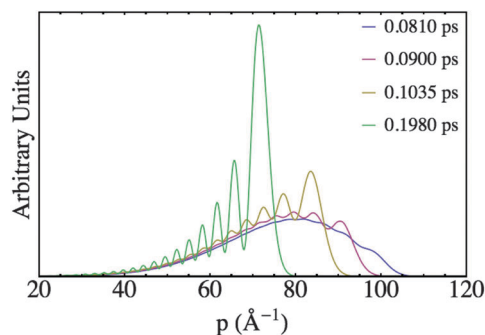


Fig. 6 Snapshots of the evolution of the squared modulus of the $\text{Cl}_2(\text{B})$ wave packet in momentum representation, showing the birth of interferences for the nanodroplet of 500 ^4He atoms.

time the largest component of $\text{WP}(p)$ (p_{max}) is released, the corresponding probability density is redistributed, in different ratios, among the lower p values at very specific distances with respect to p_{max} . This gradually leads to the formation of peaks, since the relative separations from p_{max} to the other peaks are always constant. Without the latter, the structured pattern would not be observed.

From a quantitative analysis of the resulting peaks in the probability density of $\text{WP}(p)$ at $t = 0.198$ ps (the final time of the early time photodissociation), we have determined that their positions follow a square root dependency on the order of each peak, beginning at the peak corresponding to the greatest momentum value and moving toward the peaks with lower momentum values. Hereafter, we will characterize each peak by label Δn , whose values are increasing natural numbers starting from $\Delta n = 1$. The meaning of this choice will be clear in the following discussion and a suitable representation for the peak analysis is given in Fig. 7, where the momentum of each peak is plotted as a function of $\Delta n^{1/2}$, obtaining a linear dependence.

This type of dependence, which is also evident for other times in the time period of interest, *i.e.*, not far from the early times, suggests that the mechanism to reduce the kinetic energy of the diatomic embedded molecule involves the excitation of some sort of harmonic oscillator, since the transitions are characterized by $\Delta E_{\text{oscillator}} = h\nu(n_f - n_i) \equiv h\nu\Delta n$. Therefore, by associating

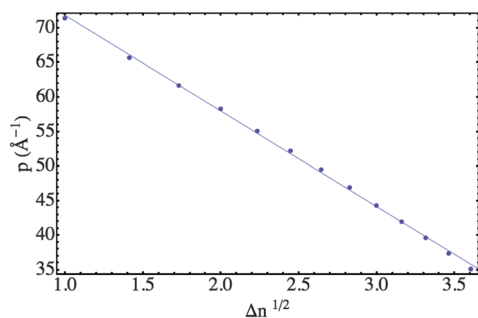


Fig. 7 Position of the peaks for the squared modulus of the $\text{Cl}_2(\text{B})$ wave packet in momentum representation at $t = 0.198$ ps as a function of $\Delta n^{1/2}$, which accounts for the number of level transitions of a harmonic quantum oscillator.

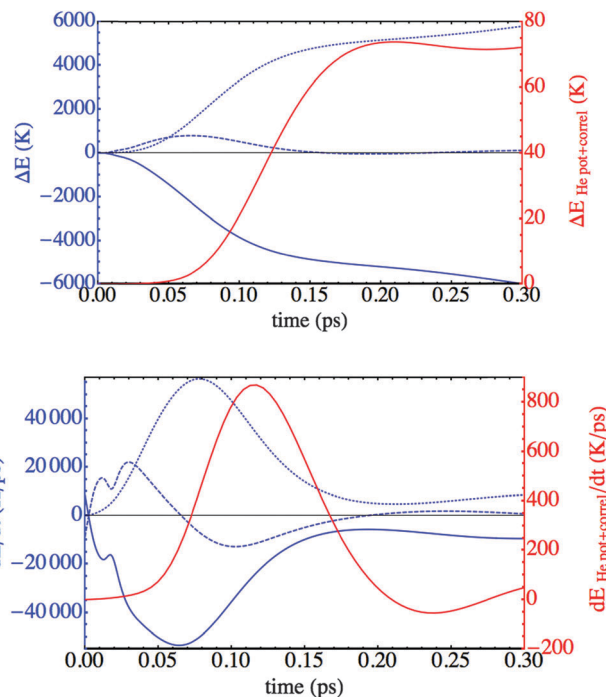


Fig. 8 Time evolution of the change of $\text{Cl}_2(\text{B})$ kinetic + potential energy (solid blue line), $\text{Cl}_2(\text{B})$ –helium interaction potential energy (dashed blue line), helium internal kinetic energy (dotted blue line), and helium internal potential + correlation energy (red) for the initial time period of the photodissociation (up). Evolution of the time derivatives of the former quantities, *i.e.*, their rates of change (down). The values reported are for $N = 500$.

a momentum value to the energy transferred, according to $p = \Delta E_{\text{oscillator}}^{1/2} \propto \Delta n^{1/2}$, each transition causes a change of momentum in $\text{WP}(p)$ from p_{max} to p_{max} minus a quantity which is proportional to $\Delta n^{1/2}$.

For deeper insights into the quantum interferences phenomenon, it is also interesting to pay attention to the energy exchanges that occur between the chlorine atoms and the helium nanodroplet, during the formation of oscillations in $\text{WP}(p)$, at the initial times of the photodissociation process. The modifications in the different energies involved with respect to their values at $t = 0$ (Table S1, ESI†) and the associated time derivatives (rates of the energy changes) are plotted in Fig. 8 for the nanodroplet with $N = 500$ and the 0.00–0.30 ps time interval and are analyzed below. Although these results correspond to $N = 500$, it should be noted that, at the early times of photodissociation, the same type of behavior is found for all the nanodroplets (*cf.* Fig. S4, ESI†).

Initially, there is an energy release from Cl_2 to the Cl_2 –helium interaction energy with monotonic rates of variation, with the exception of what happens at the very initial times, $t = 0.01$ – 0.03 ps, when small peaks are present. The rate of increase of the helium internal kinetic energy overcomes that of the interaction energy quite soon ($t = 0.034$ ps), and the energy loss of the Cl atoms and kinetic energy gain of helium continue to be accelerated until $t = 0.064$ ps and 0.078 ps, respectively. They are slightly out of phase since one is the cause of the other



and both are linked by the Cl₂-helium interaction; cf. Fig. 8 (down). The Cl₂-helium interaction energy increases with time, passes through a maximum value ($t = 0.066$ ps) and then decreases, reaching an almost constant value in the 0.16–0.24 ps time interval. Roughly speaking, the mean distance between the chlorine atoms and the cavity walls suffers a decrease and a subsequent increase. Finally, the helium internal potential + correlation energy starts to increase considerably around $t = 0.066$ ps, although it implies a much less amount of energy than the other cases, cf. the different energy scales in Fig. 8.

Hence, we can conclude that the most intense energy exchanges among the different energies involved occur at the beginning of photodissociation, $t \approx 0.00$ and 0.20 ps. Moreover, the energy changes which are more evident occur in the Cl₂ energy (kinetic + potential) and in the internal kinetic energy of helium (Fig. 8 (up)); and the significant decrease observed in the former mostly corresponds to the important increase taking place in the latter.

Regarding the interferences, it is worth noting here that the maximum increase (ΔE) in the Cl₂-helium interaction energy occurs at a time of 0.066 ps, which is similar, although smaller, to that for which the structures are observed for the first time in the $WP(p)$ probability density. A much stronger correlation is found between the maximum rate of production of helium kinetic energy ($t = 0.078$ ps; cf. Fig. 8 (down)) and the onset of structures in $WP(p)$ which occur almost at the same time. So, the quantum interferences are produced approximately when the chlorine atoms are rather separated from each other, $\langle r \rangle \approx 4.3$ Å (cf. Fig. S3, ESI† and see also the potential energy curves in Fig. 1 of ref. 4), and the displacement of the solvation shell along the photodissociation axis starts to clearly appear. Thus, the fact that the interferences seem to be the consequence of transitions of a harmonic oscillator can be related with the interaction energy. Nevertheless, the physical meaning of this is unclear.

The confinement quantum interferences found in the present theoretical study probably correspond to a rather general phenomenon in the photodissociation of molecules in superfluid helium nanodroplets, as suggested by the present study and further work in progress involving other diatomic molecules. Furthermore, it is worth noting here that oscillations in the Cl velocity distribution were also reported in ref. 10, where a different theoretical method was applied under different physical conditions (non-superfluid helium nanodroplets at $T = 4$ K with N up to 200 ⁴He atoms).

III.3 Feasibility of the experimental detection of the interferences

Regarding the experimental detection of the confinement interferences found, it is worth mentioning the significant advances achieved in recent years in the experimental techniques of chemical reactions dynamics and, in particular, in those addressed to characterize the scattering resonances,^{29–32} which are related phenomena. Accordingly, on the basis of the energy resolution needed, in principle, it should be possible to resolve

the peaks of the Cl final velocity distributions, as the separation between peaks is ≈ 46 and 56 m s^{−1} for $N = 300$ and 500 , respectively (≈ 0.38 and 0.57 meV, respectively), using imaging techniques.²⁹

Nevertheless, even though we are considering the study of a relatively simple type of chemical process that, in principle, is less complicated than the study of bimolecular reactions, which involves two pick-up steps, the experimental difficulties in order to detect the oscillations in the Cl final velocity distribution are important. This results from the technical difficulties of producing doped superfluid helium nanodroplets under well defined conditions (well defined number of ⁴He atoms, mainly).^{33,34} Unfortunately, nanodroplets are always produced with a rather wide distribution of sizes and this, obviously, will tend to blur the oscillating structures reported here. We note that for a given mean number of He atoms in the nanodroplet, \bar{N} , the width of the associated log-normal distribution, given as the full width at half maximum (FWHM), $\Delta N_{1/2}$, is comparable with \bar{N} .^{33,34}

IV. Summary and conclusions

This work extends and complements our recent investigation on the photodissociation of homonuclear diatomic molecules in superfluid helium nanodroplets ($T = 0.37$ K).⁴ In ref. 4 a hybrid theoretical method was developed and applied for the first time to investigate the photodissociation of a Cl₂ embedded molecule *via* the $B \leftarrow X$ electronic excitation: $Cl_2(X)@(^4He)_N + h\nu \rightarrow [Cl_2(B)@(^4He)_N]^* \rightarrow Cl(^2P_{3/2}) + Cl(^2P_{1/2}) + [(^4He)_{N'}]^* + (N-N') ^4He$, with $N = 50$ – 500 . This method allowed us to consider helium nanodroplets with sizes comparable to those achieved in the experiments, thus making the highly desirable connection between theory and experiment possible.

More concretely, in our theoretical study we focused on the dynamics of the process leading to the formation of confinement quantum interferences in the photodissociation of $Cl_2(B \leftarrow X)$ embedded in $(^4He)_N$. The existence of these interferences was reported but not analyzed in our previous contribution, because they were not the main target and also due to their specific character and complexity. As far as we know, this is the first time that this type of interference is described in the context of reaction dynamics.

Different from what happens in the gas phase, here the excited molecule is surrounded and provisionally confined by the helium nanodroplet and therefore a considerably longer time is required to obtain the $Cl(^2P_{3/2}) + Cl(^2P_{1/2})$ product fragments.

From the examination of the time evolution of the $Cl_2(B)$ wave packet probability density in momentum and space representations at the early times of the photodissociation (0.00 – 0.20 ps), it comes out that the interaction of $Cl_2(B)$ with the ⁴He environment generates quantum interferences. The rich structure (oscillations) produced in the Cl₂ wave function, which in the early times is much more evident in the momentum representation, is responsible of the strong oscillations which



are evident in the main observable of the system, *i.e.*, in the final velocity distribution of the Cl atoms.

These oscillations are evident for all the nanodroplets, but not for the photodissociation in the gas phase, which also clearly shows that they are caused by the interaction of Cl₂(B) with the helium environment. Moreover, a deeper insight has been obtained by paying attention to the origin of the interferences (origin and development of the oscillations in the probability density of the momentum representation wave packet) and the relationship with the energy fluxes involved.

The existence of quantum interferences is probably one of the most fascinating phenomena in chemical physics and, probably, corresponds to a quite general behavior for the kinds of systems examined. In spite of the very high technical difficulties involved in the investigation of this phenomenon, we hope that this work will encourage the experimentalists to carry out photodissociation dynamics studies on these highly interesting and challenging doped helium-4 nanodroplet systems.

Acknowledgements

This work was supported by the Spanish Ministry of Science and Innovation (projects ref. CTQ2011-27857-C02-01 and FIS2011-28617-C02-01), and we also want to acknowledge the support from the Autonomous Government of Catalonia (A. V. predoctoral fellowship and projects ref. 2009SGR 17, 2014SGR 25, 2014SGR 401 and XRQTC). We also thank Prof. Mike Ashfold (Univ. of Bristol), Prof. Peter Toennies (Max-Planck Institute, Göttingen), Prof. Alkwin Slenczka (Univ. of Regensburg), and Prof. Marcel Drabbels (EPFL, Lausanne) for very useful comments regarding the experimental techniques.

References

- 1 J. P. Toennies and A. Vilesov, Superfluid Helium Droplets: A Uniquely Cold Nanomatrix for Molecules and Molecular Complexes, *Angew. Chem., Int. Ed.*, 2004, **43**, 2622.
- 2 M. Barranco, R. Guardiola, S. Hernández, R. Mayol, J. Navarro and M. Pi, Helium Nanodroplets: An Overview, *J. Low Temp. Phys.*, 2006, **142**, 1.
- 3 S. Yang and A. M. Ellis, Helium Droplets: A Chemical Perspective, *Chem. Soc. Rev.*, 2013, **42**, 472.
- 4 A. Vilà, M. González and R. Mayol, Photodissociation Dynamics of Homonuclear Diatomic Molecules in Helium Nanodroplets. The Case of Cl₂@(⁴He)_N, *J. Chem. Theory Comput.*, 2015, **11**, 899.
- 5 S. Yang, A. M. Ellis, D. Spence, C. Feng, A. Boatwright, E. Latimer and C. Binns, Growing Metal Nanoparticles in Superfluid Helium, *Nanoscale*, 2013, **5**, 11545.
- 6 E. Latimer, D. Spence, C. Feng, A. Boatwright, A. M. Ellis and S. Yang, Preparation of Ultrathin Nanowires Using Superfluid Helium Droplets, *Nano Lett.*, 2014, **14**, 2902.
- 7 A. Braun and M. Drabbels, Photodissociation of Alkyl Iodides in Helium Nanodroplets. I. Kinetic Energy Transfer, *J. Chem. Phys.*, 2007, **127**, 114303.
- 8 A. Braun and M. Drabbels, Photodissociation of Alkyl Iodides in Helium Nanodroplets. II. Solvation Dynamics, *J. Chem. Phys.*, 2007, **127**, 114304.
- 9 A. Braun and M. Drabbels, Photodissociation of Alkyl Iodides in Helium Nanodroplets. III. Recombination, *J. Chem. Phys.*, 2007, **127**, 114305.
- 10 T. Takayanagi and M. Shiga, Photodissociation of Cl₂ in Helium Clusters: An Application of Hybrid Method of Quantum Wavepacket Dynamics and Path Integral Centroid Molecular Dynamics, *Chem. Phys. Lett.*, 2003, **372**, 90.
- 11 A. W. Hauser, A. Volk, P. Thaler and W. E. Ernst, Atomic Collisions in Suprafluid Helium Nanodroplets: Timescales for Metal-Cluster Formation Derived from He-Density Functional Theory, *Phys. Chem. Chem. Phys.*, 2015, **17**, 10805.
- 12 Y. Asano and S. Yabushita, Theoretical Study on the Non-adiabatic Transitions in the Photodissociation Processes of Cl₂, *J. Phys. Chem. A*, 2001, **105**, 9873.
- 13 N. Moiseyev, *Non-Hermitian Quantum Mechanics*, Cambridge University Press, Cambridge, 2011.
- 14 K. Liu, Quantum Dynamical Resonances in Chemical Reactions: From A + BC to Polyatomic Systems, *Adv. Chem. Phys.*, 2012, **149**, 1.
- 15 R. T. Skodje, Resonances in Bimolecular Chemical Reactions, *Adv. Quantum Chem.*, 2012, **63**, 119.
- 16 P. Gamallo, F. Huarte-Larrañaga and M. González, Resonances in the Ne + H₂⁺ → NeH⁺ + H Proton-Transfer Reaction, *J. Phys. Chem. A*, 2013, **117**, 5393.
- 17 F. Dalfvo, A. Lastri, L. Pricapenko, S. Stringari and J. Treiner, Structural and Dynamical Properties of Superfluid Helium: A Density-Functional Approach, *Phys. Rev. B: Condens. Matter Mater. Phys.*, 1995, **52**, 1193.
- 18 D. J. Tannor, *Introduction to Quantum Mechanics. A Time Dependent Perspective*, University Science Books, Sausalito, 2007.
- 19 J. Williams, A. Rohrbacher, J. Seong, N. Marianayagam, K. C. Janda, R. Burcl, M. M. Szczeniak, G. Chałasiński, S. M. Cybulski and N. Halberstadt, A Three-dimensional Potential Energy Surface for He + Cl₂(B³Π_{ou+}): Ab Initio Calculations and a Multiproperty Fit, *J. Chem. Phys.*, 1999, **111**, 997.
- 20 T. Takayanagi, private communication.
- 21 N. B. Brauer, S. Smolarek, E. Loginov, D. Mateo, A. Hernando, M. Pi, M. Barranco, W. J. Buma and M. Drabbels, Critical Landau Velocity in Helium Nanodroplets, *Phys. Rev. Lett.*, 2013, **111**, 153002.
- 22 D. Mateo, A. Hernando, M. Barranco, E. Loginov, M. Drabbels and M. Pi, Translational Dynamics of Photoexcited Atoms in ⁴He Nanodroplets: The Case of Silver, *Phys. Chem. Chem. Phys.*, 2013, **15**, 18388.
- 23 D. Mateo, F. Gonzalez and J. Eloranta, Rotational Superfluidity in Small Helium Droplets, *J. Phys. Chem. A*, 2015, **119**, 2262.
- 24 J. P. Connerade, From Pauli's Birthday to 'Confinement Resonances' – A Potted History of Quantum Confinement, *J. Phys.: Conf. Ser.*, 2013, **438**, 012001.
- 25 V. K. Dolmatov, Photoionization of Atoms Encaged in Spherical Fullerenes, *Adv. Quantum Chem.*, 2009, **58**, 13.



- 26 A. L. D. Kilcoyne, A. Aguilar, A. Muller, S. Schippers, C. Cisneros, G. Alma'Washi, N. B. Aryal, K. K. Baral, D. A. Esteves, C. M. Thomas and R. A. Phaneuf, Confinement Resonances in Photoionization of Xe@C_{60}^+ , *Phys. Rev. Lett.*, 2010, **105**, 213001.
- 27 D. R. Tilley and J. Tilley, *Condensates and Excitations. Superfluidity and Superconductivity*, Institut of Physics Publishing, Bristol, 1990, pp. 41–53.
- 28 J. F. Annet, *Superfluid Helium-4. Superconductivity, Superfluids and Condensates*, Oxford University Press, Oxford, 2004, pp. 38–43.
- 29 M. N. R. Ashfold, N. H. Nahler, A. J. Orr-Ewing, O. P. J. Vieuxmaire, R. L. Toomes, T. N. Kitsopoulos, I. Anton Garcia, D. A. Chestakov, S.-M. Wuc and D. H. Parker, Imaging the Dynamics of Gas Phase Reactions, *Phys. Chem. Chem. Phys.*, 2006, **8**, 26.
- 30 A. B. Henson, S. Gersten, Y. Shagam, J. Narevicius and E. Narevicius, Observation of Resonances in Penning Ionization Reactions at Sub-Kelvin Temperatures in Merged Beams, *Science*, 2012, **338**, 234.
- 31 C. Naulin and M. Costes, Experimental Search for Scattering Resonances in Near Cold Molecular Collisions, *Int. Rev. Phys. Chem.*, 2014, **33**, 427.
- 32 M. N. R. Ashfold and D. H. Parker, Imaging Molecular Dynamics, *Phys. Chem. Chem. Phys.*, 2014, **16**, 381. Editorial of the Imaging Molecular Dynamics themed collection (31 articles).
- 33 M. Lewerenz, B. Schilling and J. P. Toennies, A New Scattering Deflection Method for Determining and Selecting the Sizes of Large Liquid Clusters of ^4He , *Chem. Phys. Lett.*, 1993, **206**, 381.
- 34 J. Harms, J. P. Toennies and F. Dalfovo, Density of Superfluid Helium Droplets, *Phys. Rev. B: Condens. Matter Mater. Phys.*, 1998, **58**, 3341.

